

Properties of Ga-interstitial defects in $\text{Al}_x\text{Ga}_{1-x}\text{N}_y\text{P}_{1-y}$

N. Q. Thinh, I. P. Vorona,* I. A. Buyanova, and W. M. Chen†

Department of Physics and Measurement Technology, Linköping University, 58183 Linköping, Sweden

Sukit Limpijumnong

School of Physics, Institute of Science, Suranaree University of Technology, Nakhon Ratchasima 30000, Thailand

S. B. Zhang

National Renewable Energy Laboratory, Golden, Colorado 80401, USA

Y. G. Hong, H. P. Xin, and C. W. Tu

Department of Electrical and Computer Engineering, University of California, La Jolla, California 92093-0407, USA

A. Utsumi, Y. Furukawa, S. Moon, A. Wakahara, and H. Yonezu

Department of Electrical and Electronic Engineering, Toyohashi University of Technology, Toyohashi, Aichi, 441-8580, Japan

(Received 14 October 2004; published 18 March 2005)

A detailed account of the experimental results from optically detected magnetic resonance (ODMR) studies of grown-in defects in (Al)GaNP alloys, prepared by molecular beam epitaxy, is presented. The experimental procedure and an in-depth analysis by a spin Hamiltonian lead to the identification of two Ga_i defects ($\text{Ga}_i\text{-A}$ and $\text{Ga}_i\text{-B}$). New information on the electronic properties of these defects and the recombination processes leading to the observation of the ODMR signals will be provided. These defects are deep-level defects. In conditions when the defect is directly involved in radiative recombination of the near-infrared photoluminescence band, the energy level of the $\text{Ga}_i\text{-B}$ defect was estimated to be deeper than ~ 1.2 eV from either the conduction or valence band edge. In most cases, however, these defects act as nonradiative recombination centers, reducing the efficiency of light emission from the alloys. They can thus undermine the performance of potential photonic devices. High thermal stability is observed for these defects.

DOI: 10.1103/PhysRevB.71.125209

PACS number(s): 76.70.Hb, 61.72.Ji, 71.55.Eq

I. INTRODUCTION

One of the most important aspects in the physics and technology of semiconductors is to understand and control defects, which are known to often produce deep levels in the forbidden energy gap. Intrinsic defects such as self-interstitials, vacancies, and antisites have been found to be commonly occurring defects in semiconductor crystals grown under nonoptimized, nonequilibrium conditions, or subject to high-energy particle bombardment. They are fundamental building blocks for defect complexes and in some cases nucleation sites for the formation of clusters and extended defects. Intrinsic defects and their complexes are known to play a crucial role in determining the electronic and optical properties of semiconductors. In some cases when their properties are well understood and controlled, they can be used to tailor the physical properties of semiconductors such as carrier lifetime, Fermi level position, and doping [e.g., the antisite-related defects in GaAs (Refs. 1 and 2) and P_{In} antisite in InP (Refs. 3 and 4)]. In most cases, however, defects are known to severely degrade device performance and can hinder a semiconductor from practical applications. In any case, a good understanding of the defect properties is vital, especially concerning a positive identification of their chemical nature and their role in altering material properties. Up to now only very few experimental techniques have been proven successful in meeting the demand. Among them, magnetic resonance techniques have been

shown to be the most powerful of the ones that have successfully identified many intrinsic defects in semiconductors.^{5–7} When the conventional electron spin resonance (ESR) technique fails to provide the required sensitivity to reveal defects in semiconductor thin films and quantum structures grown by modern epitaxy techniques, its advanced variant—namely, the optically detected magnetic resonance (ODMR) technique—has been shown to be successful.^{8–11}

The aim of the present work is to reveal important grown-in defects in (Al)GaNP alloys by employing the ODMR technique. (Al)GaNP represents a class of newly emerging dilute nitrides, which have recently attracted great attention. These materials exhibit unusual and fascinating new physical properties, such as a giant band-gap bowing that allows widely extended band-structure engineering.^{12–19} One can also vary the lattice constant of the alloy materials over a wide range by varying the N content. For example, adding about 1.8% of N into GaP can make the parent material lattice matched to Si, opening the possibility for optoelectronic integrated circuits^{19,20} and multijunction III-V solar cells fabricated on Si wafers. A crossover from an indirect to a direct band gap induced by incorporation of $>0.4\%$ N (Refs. 15–18) promises high radiative efficiency. Due to the large mismatch in size and electronegativity between N and the replaced P atom, however, successful growth of (Al)GaNP has to be undertaken under nonequilibrium conditions.^{21,22} The nonequilibrium growth conditions, together with the disparity between N and P atoms resulting in

a strong local potential and strain field, lead to the formation of various point defects and clusters. The efficiency of visible light emissions in (Al)GaNP has been shown to deteriorate with increasing N and Al compositions. Up to now, band-to-band transitions have not been observed in this material despite the crossover to a direct band gap, due predominantly to nonradiative recombination at the defects. Currently, there is a great need in identifying important grown-in defects in this dilute nitride and in assessing their exact roles in carrier recombination.

In this work, we were able to identify Ga_i interstitial defects by ODMR as the dominant grown-in intrinsic defects in (Al)GaNP, prepared by molecular beam epitaxy (MBE). We obtained detailed information on the electronic properties of the defects and their role in carrier recombination. Preliminary results were briefly presented in a recent Rapid Communication.²³ In this paper, we shall present in details our experimental procedure and an in-depth analysis by a spin Hamiltonian that led to the identification of the two Ga_i defects. New information on the electronic properties of these defects and the recombination processes leading to the observation of the ODMR signals will be provided. A discussion about the formation mechanism of the defects will not be included here, but can be found elsewhere.²⁴ The paper is organized as follows: In Sec. II, we shall describe the samples under study, the details of the ODMR, and related photoluminescence (PL) experiments. In Sec. III, we shall present a detailed account of the ODMR results including temperature, angular, and spectral dependences. An analysis of the ODMR results by a spin Hamiltonian and a discussion of the microscopic structures of the defects and the involved recombination processes will be presented in Sec. IV. The main conclusions of the present study will be summarized in Sec. V.

II. EXPERIMENT

A. Samples

Three types of (Al)GaNP samples were studied in this work, varying by their chemical compositions and substrate materials. The first two types were grown at 520 °C on GaP substrates by gas-source molecular beam epitaxy (GS-MBE) and have a typical thickness between 0.75 and 0.9 μm. They are (1) quaternary Al_xGa_{1-x}N_yP_{1-y} with a fixed value $y=0.012$ and varied x values, $x=0.00, 0.01, 0.02,$ and 0.30 ; (2) Al-free GaN_yP_{1-y} with varied y values, $y=0.013, 0.023,$ and 0.031 . They will be referred below as AlGaNP/GaP and GaNP/GaP, respectively. The third type (denoted as GaNP/Si below) is GaN_{0.018}P_{0.982} with a thickness of 0.15 μm grown at 590 °C on a Si (100) substrate, by solid-source MBE. Rapid thermal annealing (RTA) was performed for 30 sec at the temperature range 700–900 °C with halogen lamps in a flowing N₂ ambient.

B. Experimental procedure

The ODMR measurements were performed at two microwave frequencies on a modified Bruker ER-200 D X-band (~9.3 GHz) setup with a flow cryostat and a W-band

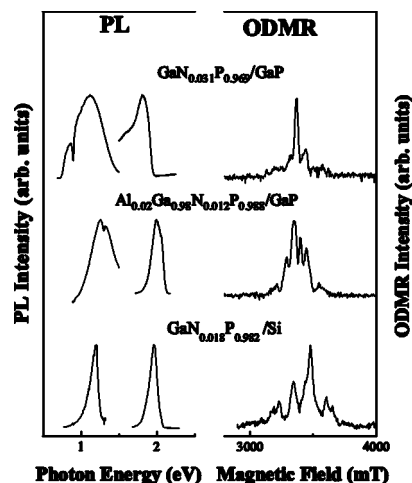


FIG. 1. Representative PL and ODMR spectra from three types of (Al)GaNP samples studied in this work. The PL spectra were measured at 2 K. The ODMR spectra were measured at 5 K and at the W band (94.8 GHz), by monitoring the NIR PL emissions. The sign of the ODMR signals is negative for GaNP/GaP and AlGaNP/GaP, but positive for GaNP/Si. They are all shown as positive for easy viewing.

(~95 GHz) setup with an Oxford superconducting split-coil magnet (0–5 T) cryostat. A solid-state laser with 532-nm wavelength was used as an excitation source in the ODMR measurements. The PL signal was detected through proper optical filters by a cooled Ge detector and a GaAs photodiode for the near-infrared (NIR) and visible spectral range, respectively. The ODMR signals were detected by the lock-in technique as spin-resonance-induced changes of PL intensity, in phase with an amplitude modulation (0.5–20 kHz) of the microwave radiation. The typical microwave power employed was 170–200 mW. The measurements were performed in the temperature range of 2–40 K.

III. RESULTS

A. PL and ODMR

Upon above-band-gap optical excitation, all three types of the samples studied exhibit PL emissions in the visible spectral range (see Fig. 1) that are known to arise from N-related localized states.²⁵ They also give rise to defect-related deep PL emissions within the NIR spectral range whose origins are still largely unknown (see the PL bands at the lower energies in Fig. 1). Judging from their energy positions and their shifts with N and Al compositions, as well as different signs of the ODMR signals (to be presented below), we believe that the deep emissions from the three types of samples are of different origins. Representative PL spectra from the three types of samples are given in Fig. 1, together with typical ODMR spectra obtained by monitoring these PL emissions. The ODMR spectra show the following two distinct features originated from different defects. The first one is a single strong line situated in the middle of the ODMR spectra from the AlGaNP/GaP and GaNP/GaP samples, with a g value close to 2. Due to a lack of hyperfine (HF) structure, unfortunately, the chemical nature of the corre-

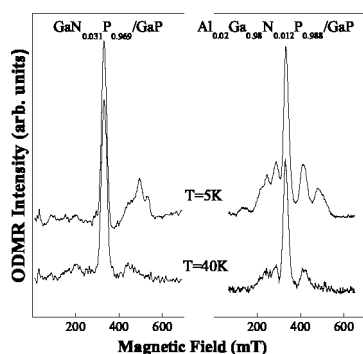


FIG. 2. ODMR spectra taken at two different temperatures, 5 and 40 K, from $\text{GaN}_{0.031}\text{P}_{0.969}/\text{GaP}$ and $\text{Al}_{0.02}\text{Ga}_{0.98}\text{N}_{0.018}\text{P}_{0.982}/\text{GaP}$. The X-band microwave frequency was 9.31 GHz.

sponding defect cannot be identified. Below we shall simply refer to it as the “ $g=2$ ” defect. The second feature of the ODMR spectra consists of a complicated pattern of lines spreading over a wide field range. Such multiple ODMR lines can arise from a high-electron-spin state exhibiting a zero-field splitting due to a defect crystal field, from an HF interaction involving a high nuclear spin, or from several overlapping ODMR signals due to different defects. To resolve this issue, the temperature and angular dependences of the ODMR spectra were investigated.

B. Temperature dependence of the ODMR

To examine if the second feature of the ODMR spectra originates from a single or more than one defect, temperature dependence studies were performed. This is because the temperature dependence of spin-lattice relaxation is often different, such that relative intensity of the ODMR signals from different defects may be altered by the measurement temperature. ODMR spectra from AlGaNP/GaP and GaNP/GaP at 5 K and 40 K (Fig. 2) clearly show that about half of the multiple ODMR lines undergo thermal quenching in intensity. This finding provides strong evidence that the multiline feature of the ODMR spectra in fact consists of two groups of lines from two different defects (denoted as $\text{Ga}_i\text{-A}$ and $\text{Ga}_i\text{-B}$), of which $\text{Ga}_i\text{-B}$ loses signal strength at elevated temperatures and vanishes at $T \geq 40$ K (see Fig. 2).

C. Angular dependence of the ODMR

Both $\text{Ga}_i\text{-A}$ and $\text{Ga}_i\text{-B}$ give rise to multiple ODMR lines, which can arise either from a high-electron-spin state exhibiting a zero-field splitting caused by a defect crystal field or from an HF interaction involving a high nuclear spin. The former should give rise to an anisotropic ODMR spectrum reflecting the symmetry of the defect, whereas the latter may or may not do so. To identify the origin of the multiple ODMR lines, angular dependence studies were carried out by rotating the external magnetic field in a $\{110\}$ crystallographic plane. Typical ODMR spectra are displayed in Fig. 3 when the direction of the external magnetic field is oriented along the three main crystallographic axes, as examples. The ODMR spectra are shown to be isotropic, within the experi-

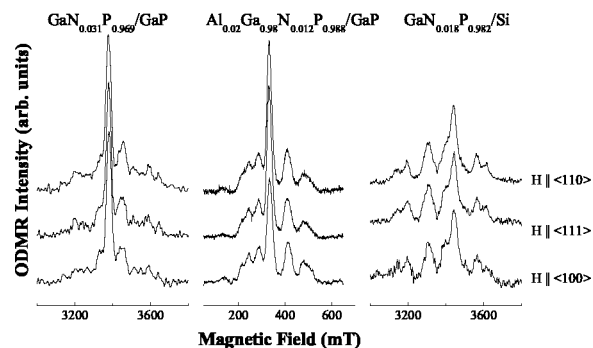


FIG. 3. ODMR spectra of the three types of $(\text{Al})\text{GaNP}$ samples obtained at 5 K and when the external magnetic field was oriented along the three main crystallographic axes. The $\text{Al}_{0.02}\text{Ga}_{0.98}\text{N}_{0.018}\text{P}_{0.982}/\text{GaP}$ sample was measured at the X band, while the other two samples were measured at the W band.

mental error. This finding supports the assignment that the multiple ODMR lines for each defect should be due to an HF structure, which will be shown below to arise from a strong interaction between an unpaired electron spin ($S=1/2$) and the nuclear spin ($I=3/2$) of a Ga atom.

D. Spectral dependence of the ODMR

In the AlGaNP/GaP and GaNP/GaP samples, all defects—i.e., the “ $g=2$ ” defect, the $\text{Ga}_i\text{-A}$, and the $\text{Ga}_i\text{-B}$ —give rise to negative ODMR signals that correspond to a decrease upon spin resonance in the intensity of the monitored PL emissions over the entire visible and NIR spectral range. (The ODMR signals are displayed as positive ones throughout the paper merely for easy viewing.) The only exception occurs for the $\text{Al}_x\text{Ga}_{1-x}\text{N}_y\text{P}_{1-y}$ sample series when $x=0.00$ and $y=0.012$, where the sign of the ODMR signals turns to positive by monitoring the NIR PL emissions. A possible reason for this sign change will be discussed in Sec. IV E. In the GaNP/Si samples, however, the ODMR signals (shown in Figs. 1 and 3) correspond to a spin-resonance-induced increase in the monitored NIR PL emission—i.e., a positive sign of ODMR. On the other hand, in the visible spectral range, the ODMR signal strength was too weak to be detected.

E. Effect of RTA on the ODMR

In Fig. 4, we show representative ODMR spectra from the AlGaNP alloys before and after post-growth RTA treatments. All the defects under study exhibit high thermal stability up to 900 °C and can only be partially removed by RTA. It should be noted that the RTA causes a larger reduction of the “ $g=2$ ” defect than the two Ga_i defects.

IV. DISCUSSION

A. Spin Hamiltonian analysis

The left panels of Figs. 5–7 show that the ODMR spectra at the X band are rather irregular, which makes it very difficult to assign them to a specific nuclear spin state. For this reason, the ODMR was also performed at the W band in a

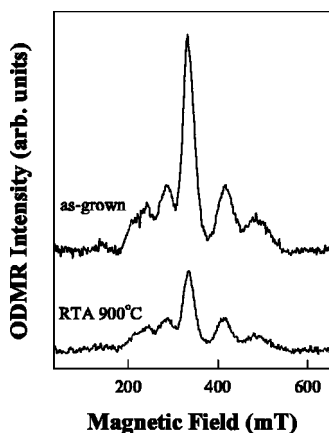


FIG. 4. ODMR spectra from the as-grown and RTA treated $\text{Al}_{0.02}\text{Ga}_{0.98}\text{N}_{0.018}\text{P}_{0.982}/\text{GaP}$ samples, obtained at 5 K for the X band. The RTA treatment was done at 900 °C.

higher magnetic field, which usually avoids a strong nonlinear Zeeman effect due to level repelling at low fields. The ODMR spectra at the *W* band show a clear pattern with two groups of lines from $\text{Ga}_7\text{-A}$ and $\text{Ga}_7\text{-B}$ with distinctly different intensities. Each defect shows grossly four lines with additional features (a shoulder or a splitting). A close inspection reveals that each defect in fact gives rise to two sets of four lines with a fixed intensity ratio of 40/60 and a fixed ratio of line spacing=1.3. The most plausible explanation for these experimental findings is that the ODMR lines from each defect should originate from the HF structure related to an atom with the following properties: (i) it has two isotopes, of which both have a nuclear spin $I=3/2$ to account for the two sets of four lines; (ii) the ratio of the natural abundances of the two isotopes should be near 40/60 to account for the ratio of the corresponding ODMR intensity; (iii) the ratio of the nuclear magnetic moments of the two isotopes should be near 1.3 to account for the ratio of the line spacing.

To confirm the assignment and to obtain information on the physical properties of the defects, a detailed analysis of the experimental data was performed using the following spin Hamiltonian:

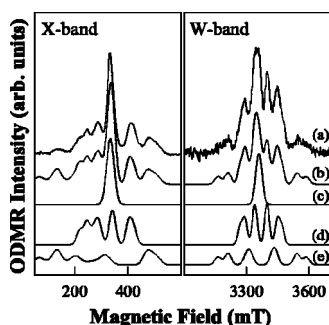


FIG. 5. (a) Experimental ODMR spectra from $\text{Al}_{0.02}\text{Ga}_{0.98}\text{N}_{0.018}\text{P}_{0.982}/\text{GaP}$, taken at 5 K for both the X (9.31 GHz) and *W* (94.8 GHz) bands. (b) The simulated ODMR spectra including contributions from (c)–(e) below. (c) The simulated ODMR spectrum for the “ $g=2$ ” defect. A fitting value of $g=2.017$ was used. (d) and (e) The simulated ODMR spectra for $\text{Ga}_7\text{-A}$ and $\text{Ga}_7\text{-B}$, respectively, by using the spin Hamiltonian parameters given in Table I.

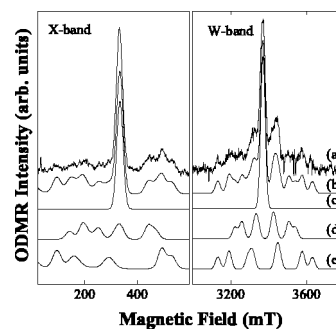


FIG. 6. (a) Experimental ODMR spectra from $\text{GaN}_{0.031}\text{P}_{0.969}/\text{GaP}$, taken at 5 K at both the X (9.31 GHz) and *W* (94.8 GHz) bands. (b)–(e) have the same meaning as in Fig. 5.

$$H = \mu_B \mathbf{B} \cdot \mathbf{g} \cdot \mathbf{S} + \mathbf{S} \cdot \mathbf{A} \cdot \mathbf{I}. \quad (1)$$

Here the first and second terms describe electron Zeeman and central HF interactions, respectively; μ_B is the Bohr magneton, \mathbf{B} is the external magnetic field, \mathbf{g} is the Zeeman splitting tensor, and \mathbf{A} is the central HF interaction tensor for each isotope. The effective electron spin is $S=1/2$ and the nuclear spin is $I=3/2$. By fitting the spin Hamiltonian to the experimental data, the spin Hamiltonian parameters were determined for both $\text{Ga}_7\text{-A}$ and $\text{Ga}_7\text{-B}$ in all samples and are given in Table I. Both \mathbf{g} and \mathbf{A} tensors are deduced to be isotropic, within the experimental accuracy, and are reduced to the scalars g and A . This finding, together with the rather strong HF interaction, points to A_1 symmetry (*s* like) for the electron wave function localized at the defects. For example, Figs. 5–7 show the simulated ODMR curves for $\text{Al}_{0.02}\text{Ga}_{0.98}\text{N}_{0.012}\text{P}_{0.988}/\text{GaP}$, $\text{GaN}_{0.031}\text{P}_{0.969}/\text{GaP}$, and $\text{GaN}_{0.018}\text{P}_{0.982}/\text{Si}$, assuming a Gaussian line shape for each ODMR line. It is apparent that the agreement between the simulations and the experimental results is very good for both *X*- and *W*-band spectra.

The intensity of the low-field *X*-band ODMR lines appears to be weaker in experiment than in simulation. This can be attributed to the fact that the simulations only take into account magnetic-dipole-allowed electron spin resonance transitions but not the difference in recombination rates of the spin sublevels.^{10,11} At lower fields when the electronic Zeeman term becomes comparable or weaker than the

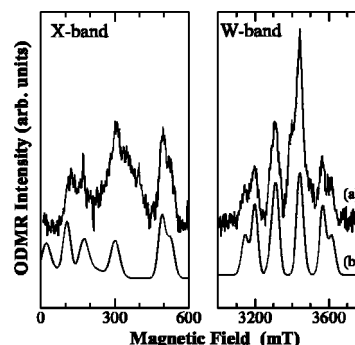


FIG. 7. (a) Experimental ODMR spectra from $\text{GaN}_{0.018}\text{P}_{0.982}/\text{Si}$, taken at 5 K at both the X (9.31 GHz) and *W* (94.8 GHz) bands. (b) The simulated ODMR spectra for $\text{Ga}_7\text{-B}$.

TABLE I. Spin Hamiltonian parameters determined by fitting Eq. (1) to experimental data for the Ga_i - A and Ga_i - B defects in the three types of samples. Spin density η^2 at Ga_i is also shown and is deduced from our calculated $4s$ electron density, $|\psi_{4s}(0)|^2 = 72.7 \times 10^{24} \text{ cm}^{-3}$. Note that for the $GaN_{0.018}P_{0.982}/Si$ and $Al_xGa_{1-x}N_yP_{1-y}/GaP$ ($x=0$ and $y=0.012$) samples, the ODMR signal of Ga_i - A , if existing, is obscured by the presence of the much stronger ODMR signals from other defects and thus its HF interaction parameter cannot be reliably determined. No ODMR signals from Ga_i - A and Ga_i - B were observed in the $GaN_{0.013}P_{0.987}/GaP$ sample within the detection limit of our ODMR experiments.

Samples	GaN_yP_{1-y}/GaP				GaN_yP_{1-y}/Si		$Al_xGa_{1-x}N_yP_{1-y}/GaP$						
	0		0.023		0	0	0.01		0.02		0.3		
x													
y	0.031		0.023		0.018				0.012				
Defect	Ga_i - A	Ga_i - B	Ga_i - A	Ga_i - B	Ga_i - B	Ga_i - B	Ga_i - A	Ga_i - B	Ga_i - A	Ga_i - B	Ga_i - A	Ga_i - B	
S	1/2	1/2	1/2	1/2	1/2	1/2	1/2	1/2	1/2	1/2	1/2	1/2	1/2
I	3/2	3/2	3/2	3/2	3/2	3/2	3/2	3/2	3/2	3/2	3/2	3/2	3/2
g	2.001	2.003	2.001	2.003	2.001	2.005	2.01	2.005	2.01	2.005	2.01	2.005	2.01
$A(^{69}Ga) \times 10^{-4} \text{ cm}^{-1}$	770	1150	770	1150	1145	1150	490	1030	490	1030	450	980	
$A(^{71}Ga) \times 10^{-4} \text{ cm}^{-1}$	1000	1480	1000	1480	1477	1480	630	1320	630	1320	580	1260	
$\eta_2(Ga_i)$	0.20	0.30	0.20	0.30	0.30	0.30	0.13	0.27	0.13	0.27	0.12	0.25	

HF interaction [see Eq. (1)], the spin sublevels undergo strong admixing due to the HF interaction, which reduces the difference in the recombination rates. As the ODMR intensity is proportional^{10,11} to the product of the microwave-induced spin transition probability and the difference in the recombination rates, a reduction of the latter should thus lead to a decrease in the actual ODMR intensity.

It should also be noted that the fitting of the ODMR spectra from the $GaN/P/Si$ samples in Fig. 7 is less satisfactory by considering Ga_i - B alone, due to a contribution from a broad background close to the middle of the spectra. Though a contribution from Ga_i - A to the background is possible, it cannot be definitely concluded since the characteristic HF structure was not resolved in this case. Even assuming the contribution from Ga_i - A , additional contributions from other unknown defect(s) are still apparent. A similar situation occurs in the Al-free sample in the $AlGaNP/GaP$ series—i.e., the only other sample that also exhibits positive ODMR signals. In both cases, the strong ODMR line related to the “ $g=2$ ” defect, which dominates the ODMR spectra in the rest of the samples, is absent.

B. Defect identification

The above analysis proves that both Ga_i - A and Ga_i - B involve an atom with well-defined natural abundances of the two isotopes and their respective nuclear spin numbers and magnetic moments. Among all elements, only Ga meets all these specifications. Ga has two naturally abundant isotopes: ^{69}Ga (60.4% abundant) and ^{71}Ga (39.6% abundant). The ratio of their nuclear magnetic moments is $\mu(^{71}Ga)/\mu(^{69}Ga) = 1.27$. Our ODMR results thus provide compelling evidence for the involvement of a Ga atom in the core of both Ga_i - A and Ga_i - B defects.

Now let us turn to the location of the Ga atom in Ga_i - A and Ga_i - B that gives rise to the observed HF structure. A Ga atom, instead of residing in its designated lattice site, can reside either on a site of the group-V sublattice forming a cation antisite or on an interstitial position leading to Ga

self-interstitials. A Ga-related cation antisite was predicted by earlier²⁶ and our present theoretical calculations to possess an electron wave function of T_2 symmetry, which will yield a very weak and anisotropic HF interaction at the defect center. This is clearly inconsistent with our experimental observation of the strong isotropic HF interaction and can therefore be ruled out as a candidate for the model of Ga_i - A and Ga_i - B under study. Our theoretical calculations also estimate that the HF interaction of a neutral Ga_i should be weaker than $100 \times 10^{-4} \text{ cm}^{-1}$, which cannot explain the observed strong HF interaction. A Ga_i in its Ga_i^{2+} charge state, on the other hand, is predicted to possess a strongly localized electron wave function of A_1 symmetry in agreement with the experimental results. Therefore we can conclude that the Ga atom in the Ga_i - A and Ga_i - B defects is a Ga_i^{2+} interstitial.

The next question is whether both Ga_i - A and Ga_i - B are just simple, isolated Ga_i residing on different Ga_i sites or Ga_i -related complexes. For that we calculated for each microscopic configuration the HF interaction A from the interaction between the spin density of the electron and the nuclear spins. Using state-of-the-art first-principles supercell calculations as implemented in the WIEN2k code,²⁷ we calculated the electron spin distribution topology that was then used to calculate the HF tensor. The calculations were based on generalized gradient approximations (GGA's) within the framework of density functional theory (DFT), using the all-electron full-potential linearized augmented-plane-wave (FP-LAPW) method. The relativistic effects were included through a scalar relativistic treatment for valence electrons. All atoms in the supercell are allowed to relax. The atomic geometry optimization has been performed using the first-principles ultrasoft pseudopotential plane-wave method with GGA as implemented in the VASP code.²⁸ Our test calculations of a well-established signature, Zn_i in $ZnSe$,²⁹ yielded the central HF parameter in good agreement with the experiment to within 10%. A supercell containing 32 atoms, which was sufficient to provide converged HF parameters,³⁰ was used. The electron density of a free atom was calculated by

placing the atom in a large cubic supercell ($10 \times 10 \times 10 \text{ \AA}^3$) to reduce the intercell interactions. Our theoretical calculations predict strong HF interactions for isolated Ga_i in GaP: i.e., $A(^{69}\text{Ga}) = 1876 \times 10^{-4} \text{ cm}^{-1}$ for Ga_i at the T_d site surrounded by four Ga atoms and $A(^{69}\text{Ga}) = 1599 \times 10^{-4} \text{ cm}^{-1}$ for Ga_i at the T_d site surrounded by four P atoms. These values are much larger ($>30\%$) than the experimental values determined for Ga_i -A and Ga_i -B. A reduced HF interaction is commonly regarded as evidence for a complex due to charge transfer or redistribution of the electron wave function from Ga_i to the other partner(s) of the complex. This conclusion is supported by recent experimental ODMR studies in wurtzite GaN that have convincingly shown that isolated Ga self-interstitials are unstable at temperatures well below room temperature and readily form complexes.^{31–33} Considering the more dilute crystal lattice of the GaNP and AlGaNP alloys that makes Ga_i easier to migrate, the isolated Ga self-interstitials in these alloys are more likely to be unstable at the growth temperatures, leading to the formation of complexes. Such complexes usually possess larger binding energies, which are consistent with the observed high thermal stability of the Ga_i -A and Ga_i -B defects.

C. Localization of electron wave functions at the defects

The degree of localization of the electron wave functions at the defect can be estimated using a one-electron linear combination of atomic orbital (LCAO) scheme.³⁴ The wave function for the unpaired electron can be constructed as a LCAO centered on the atoms surrounding the defect:

$$\Psi = \sum_i \eta_i \psi_i. \quad (2)$$

The wave function on the i th site can be approximated as a hybrid of the ns , np orbitals:

$$\psi_i = \alpha_i (\psi_{ns})_i + \beta_i (\psi_{np})_i, \quad (3)$$

where $n=4$ for Ga. The normalization, ignoring the overlap, requires

$$\alpha_i^2 + \beta_i^2 = 1, \quad \sum_i \eta_i^2 = 1. \quad (4)$$

Generally, with an axially symmetric A tensor, the principal values can be described as

$$A_{\parallel}^i = a_i + 2b_i, \quad (5)$$

$$A_{\perp}^i = a_i - b_i, \quad (6)$$

where

$$a_i = \frac{8}{3} \pi g_0 g_N \mu_B \mu_N \alpha_i^2 \eta_i^2 |\psi_{4s}(0)|_i^2, \quad (7)$$

$$b_i = \frac{2}{5} g_0 g_N \mu_B \mu_N \beta_i^2 \eta_i^2 \langle r_{3p}^{-3} \rangle_i. \quad (8)$$

Here g_0 and g_N denote electron and nuclear g values. In our case, the HF tensor of the Ga_i site is shown to be isotropic—

i.e., $A_{\parallel}^{\text{Ga}} = A_{\perp}^{\text{Ga}}$ and thus $\alpha_{\text{Ga}}^2 = 1$ and $\beta_{\text{Ga}}^2 = 0$. The wave function of the unpaired electron at the Ga_i -A and Ga_i -B defects can then be approximated as being constructed from the s orbital only.

For a free neutral Ga atom, we calculated the charge density of the $4s$ electron using the relativistic GGA-FP-LAPW method described in Sec. IV B and found $|\psi_{4s}(0)|^2 = 72.7 \times 10^{24} \text{ cm}^{-3}$. Based on this, we estimate the localization of the unpaired electron at the Ga_i to be in the range of 12%–30% (Table I). The rather strong localization confirms that these are deep-level defects.

D. Local surrounding of the defects

In a tetrahedral semiconductor like GaNP or AlGaNP, self-interstitials can occupy three high-symmetry positions in which two of them have T_d symmetry surrounded by group-III or group-V atoms, respectively, and the third has hexagonal symmetry (D_{3d}) surrounded by both group-III and group-V sublattices. In order to provide information on the specific Ga_i site and the sublattice immediately surrounding the Ga_i in Ga_i -A and Ga_i -B, the chemical compositions of each sublattice were varied experimentally by varying Al and N compositions. The results are summarized in Table I. It can be seen that a rather strong reduction (about 10% for Ga_i -B) of the HF interaction was observed when the Al composition is raised from $x=0.00$ to as low as $x=0.01$. With a further increase in Al composition, however, the rate of decrease in the HF interaction is drastically reduced to about 5% from $x=0.01$ to $x=0.30$. This observation indicates that Al directly affects the Ga_i -A and Ga_i -B defects. The nonlinear dependence also indicates that the presence of Al near the defects may not necessarily follow the statistic distribution expected for random alloy formation.²⁴ This suggestion is further supported by the fact that the ODMR intensity increases significantly upon incorporation of Al in the alloy. We should point out that the incorporation of Al in GaAs was also required to introduce the Ga_i defect in AlGaAs.^{35,36} Moreover, the strength of the HF interaction in the (Al,Ga)As-based structures^{35–38} is very close to that of Ga_i -A in the Al-containing AlGaNP studied in this work. Assuming that a similar Ga_i defect complex is involved, the correlation between these two alloy systems seems to suggest that the Ga_i in Ga_i -A is surrounded by the group-III sublattice as the group-V sublattice is made of completely different atoms between AlGaAs and AlGaNP. In the previous studies of Ga_i in AlGaAs,³⁵ it was suggested that Ga_i is not very near the group-III sublattice based on the experimental observation that the ODMR spectrum is insensitive to the change of Al composition from 20% to 50%. Our finding of the nonlinear dependence of the HF interaction on Al compositions, which exhibits a much-reduced variation for high Al compositions, questions this earlier suggestion.

In contrast to the dependence on Al composition, the HF interaction of both Ga_i -A and Ga_i -B defects in GaNP was found in this work to be insensitive to N compositions up to 3%. On the other hand, the incorporation of N is essential for the observation of the Ga_i -A and Ga_i -B defects in

GaNP. This indicates that either N is directly involved as part of the defect or the required nonequilibrium growth conditions or possible ion bombardment during the incorporation of N in GaNP facilitates the formation of the Ga_i-A and Ga_i-B defects. It is interesting to note that the strength of the HF interaction of Ga_i-A in GaNP, $A(^{69}\text{Ga})=770 \times 10^{-4} \text{ cm}^{-1}$, is very close to $741 \times 10^{-4} \text{ cm}^{-1}$ observed for the Ga_i in its parent GaP.³⁹ The same applies to Ga_i-A in AlGaNP; i.e., $A(^{69}\text{Ga})=(450-490) \times 10^{-4} \text{ cm}^{-1}$ is very close to $500 \times 10^{-4} \text{ cm}^{-1}$ observed in the AlGaAs-based alloys.³⁵⁻³⁸ In contrast, Ga_i-B was never observed in N-free GaP and AlGaAs-based alloys. This may indicate that N could be directly involved in the structure of the Ga_i-B defect.

E. Recombination processes

The ODMR signals were detected as changes of the PL intensity induced by the spin resonance. The sign of the ODMR signals can thus provide us with useful information about the role of the involved defects in carrier recombination processes.

In the GaNP/GaP series of samples, in Figs. 1 and 6, the ODMR signals correspond to a decrease upon spin resonance in the intensity of all monitored PL emissions over the entire spectral range. Such a negative and emission-insensitive ODMR signal has often been taken as a signature of a nonradiative defect,^{10,39} which is not directly related to the monitored PL emissions. The reason why a nonradiative defect can be detected via a radiative recombination process lies on their competition in recombination of photogenerated free carriers. Figure 8(a) shows schematically the recombination processes leading to the observation of the negative ODMR signals. Spin-resonance-enhanced recombination via a nonradiative defect leads to a reduction of free carriers available for radiative recombination and thus to a decrease in the intensity of PL emissions.^{10,11,25,40} Such nonradiative recombination can occur via a single defect or via intercenter charge transfer⁴¹ between two defects—e.g., between the “g=2” defect and Ga_i-A (or Ga_i-B). The latter scenario is quite likely in the present case, judging from the simultaneous appearance of these two defects for each sample under various measurement conditions. Therefore it can be concluded that Ga_i-A, Ga_i-B, and the “g=2” defect act as nonradiative recombination channels, reducing the radiative efficiency of the alloys. This is confirmed by an anticorrelation between the intensities of the visible PL emissions and the ODMR signals, in Fig. 9. For example, a significant increase in the ODMR intensity of the Ga_i-A and Ga_i-B defects (and also the “g=2” defect) can be observed with increasing N composition, which is accompanied by a substantial decrease of the visible PL emissions. These defects can undermine performance of potential photonic and optoelectronic devices and therefore should be addressed adequately. The observed increase of the NIR PL in Fig. 9, on the other hand, can be explained by the fact that the NIR PL originates from defects that were introduced by the incorporation of N.

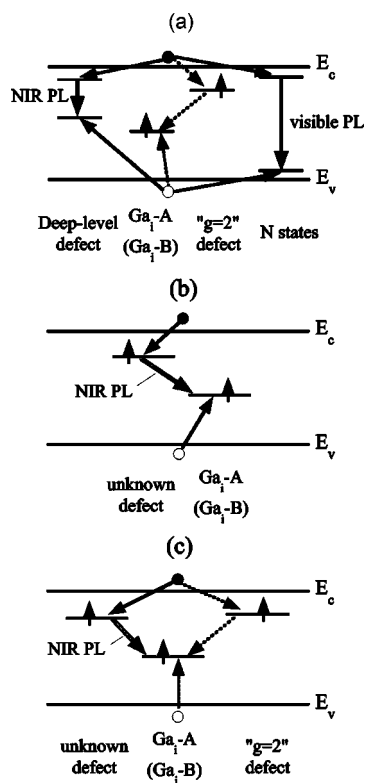


FIG. 8. (a) A schematic diagram of the carrier recombination processes leading to the observation of negative ODMR signals in GaNP/GaP. The spin resonance induces an increase in the nonradiative recombination (indicated by the dashed arrows) via the “g=2” and Ga_i-A (or Ga_i-B) defects and a decrease in the radiative recombination process monitored by the PL in both the visible and NIR spectral ranges. (b) A schematic diagram of the carrier recombination process leading to the observation of positive ODMR signals in GaNP/Si; i.e., the spin-resonance-induced increase in the radiative recombination via the unknown defect and Ga_i-A (or Ga_i-B) is directly monitored by the NIR PL. (c) A schematic diagram of the competitive carrier recombination processes leading to the observation of positive and negative ODMR signals in the AlGaNP/GaP series of samples.

In the GaN_{0.018}P_{0.982}/Si samples, the ODMR signals were found to be positive by monitoring the NIR PL emissions (Figs. 1 and 7). This can be explained as follows: The monitored PL emission is directly related to the defects—e.g., intercenter charge transfer between an unknown defect and the Ga_i-A (or Ga_i-B) defect [see Fig. 8(b)]. The spin-resonance-enhanced radiative recombination between them leads to an intensity increase of the corresponding PL. It should be pointed out that the “g=2” defect is absent in this case. Instead, a broad background ODMR was detected, as shown in Fig. 7, of which the origin of the corresponding defect is still unknown. It is denoted as “unknown defect” in Fig. 8(b). The energy of the related PL emission can usually be employed to estimate the energy position of the defect level if the recombination process is fully understood. Since the spin-dependent recombination processes involving the Ga_i defects are likely to be of an intercenter charge transfer origin and the energy position of the other partner is unknown, at present we are not able

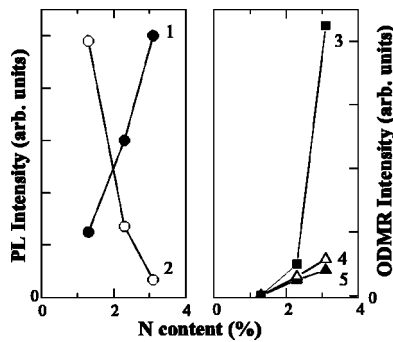


FIG. 9. Relative intensities of the PL emissions and the ODMR signals as a function of the N composition, obtained from the GaNP/GaP series of samples. The open and solid circles denote the intensities of the visible and NIR PL emissions, respectively. The solid and open triangles represent the intensities of the Ga_i-A and Ga_i-B ODMR signals, respectively. The solid squares denote the ODMR intensity of the “ $g=2$ ” defect.

to precisely deduce the energy level positions of the Ga_i defects. However, a rough estimate of the energy position for the Ga_i-B defect can be made to be at least >1.2 eV away from either the conduction or valence band edge.

In the AlGaNP/GaP series of samples, on the other hand, both positive and negative ODMR signals have been observed, depending on the Al compositions and the monitored PL. In the Al-free sample, positive ODMR signals similar to that from the GaN_{0.018}P_{0.982}/Si sample were detected by monitoring the NIR PL. The recombination process can thus be described in a similar fashion as discussed above and shown in Fig. 8(b). In the Al-containing AlGaNP, however, the ODMR signals switch sign to become negative. This is accompanied by the appearance of the “ $g=2$ ” defect and a simultaneous disappearance of the “unknown defect” in the ODMR spectra, as shown in Fig. 5. This sign change can be understood, as schematically shown in Fig. 8(c), by the following competing intercenter charge transfer and recombination processes between these defects: (1) the nonradiative recombination between the “ $g=2$ ” and Ga_i-A (or Ga_i-B) defects, which gives rise to negative ODMR signals, and (2) the radiative recombination between the “unknown defect” and the Ga_i-A (or Ga_i-B) defect, which gives rise to positive ODMR signals. In principle, both processes coexist and the sign of the combined ODMR signals depends on their relative importance. The change of the signal sign from positive in the Al-free sample to negative in the Al-containing samples as soon as Al is incorporated suggests that process (1) becomes dominant over process (2). With increasing Al composition, the intensity of the negative ODMR signals in Fig. 10 increases, signifying the importance of the nonradiative recombination between the “ $g=2$ ” and Ga_i-A (or Ga_i-B) defects. With a further increase of the Al composition to 30%, however, the ODMR intensity decreases for all defects. This is a sign that other nonradiative defects become important and overshadow the above defects.

It should be pointed out that, although the intercenter charge transfer is shown in Fig. 8 only from the “ $g=2$ ” de-

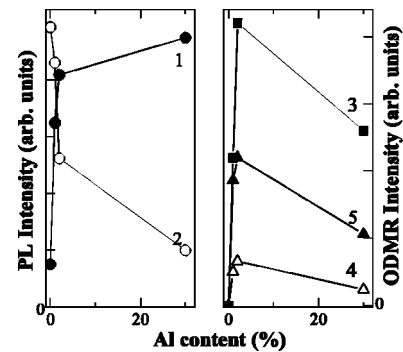


FIG. 10. Relative intensities of the PL emissions and the ODMR signals as a function of the Al composition, obtained from the AlGaNP/GaP series of samples. The legends are the same as in Fig. 9.

fect (or the “unknown defect”) to the Ga_i-A (or Ga_i-B) defect, the reverse process is also possible if their energy order is reversed. This possibility holds as long as the paramagnetic charge state of Ga_i in the Ga_i-A (or Ga_i-B) defect, before the charge transfer, is 2+.

V. CONCLUSIONS

In summary, we have studied and identified two different Ga_i defects in dilute nitride AlGaNP by ODMR. The assignment of Ga_i to both defects is concluded from its unique HF interaction. Both defects are complexes involving a Ga_i²⁺. The redistribution of the electron wave function leads to a reduction of the HF interaction. The HF interaction also strongly depends on the presence of Al, indicating that the defects may be surrounded by group-III atoms. The incorporation of both Al and N is shown to play an important role in the formation of the defects, indicative of the involvement of N in Ga_i-B. The defects are found to introduce energy levels deep inside the band gap—e.g., ~ 1.2 eV from the conduction (or valence) band edge for the Ga_i-B defect. In most cases, these defects act as nonradiative recombination centers reducing the efficiency of light emissions from the alloys. They can thus undermine the performance of photonic devices based on these materials. In view of the high thermal stability (at up to 900 °C) of the defects, post-growth RTA was found to be inadequate to remove the defects. Future studies are needed to control their formation during the growth, in order to improve radiative efficiency. The present studies also shed new light on Ga self-interstitials in III-V’s in general.

ACKNOWLEDGMENTS

The financial support by the Swedish Research Council and the Wenner-Gren Foundations is greatly appreciated. The work at NREL was supported by the U.S. DOE/BES and DOE/EERE under Contract No. DE-AC36-99GO10337. The work in Thailand was supported by the Thailand Research Fund under Contract No. BRG4680003 and by the AFOSR/AOARD under Contract No. AOARD-05-4013.

- *Permanent address: Institute of Semiconductor Physics, Pr. Nauky 45, Kiev 03028, Ukraine.
- †Corresponding author: wmc@ifm.liu.se
- ¹G. M. Martin and S. Makram-Ebeid, in *Deep Centers in Semiconductors*, edited by S. Pantelides (Gordon and Breach, New York, 1986), p. 389.
 - ²X. Liu, A. Prasad, W. M. Chen, A. Kurpiewski, A. Stoschek, Z. Liliental-Weber, and E. R. Weber, *Appl. Phys. Lett.* **65**, 3002 (1994).
 - ³W. M. Chen, I. A. Buyanova, A. Buyanov, T. Lundström, W. G. Bi, and C. W. Tu, *Phys. Rev. Lett.* **77**, 2734 (1996).
 - ⁴W. M. Chen, P. Dreszer, A. Prasad, A. Kurpiewski, W. Walukiewicz, E. R. Weber, E. Sörman, B. Monemar, B. W. Liang, and C. W. Tu, *J. Appl. Phys.* **76**, 600 (1994).
 - ⁵G. D. Watkins, *Semicond. Semimetals* **51A**, 1 (1998).
 - ⁶J.-M. Spaeth, J. R. Niklas, and R. H. Bartram, *Structural Analysis of Point Defects in Solids* (Springer-Verlag, New York, 1992).
 - ⁷U. Kaufmann and J. Schneider, *Festkoerperprobleme* **20**, 87 (1980).
 - ⁸B. C. Cavenett, *Adv. Phys.* **30**, 475 (1981).
 - ⁹T. A. Kennedy and E. R. Glaser, *Semicond. Semimetals* **51A**, 93 (1998).
 - ¹⁰W. M. Chen, *Thin Solid Films* **364**, 45 (2000).
 - ¹¹W. M. Chen, in *EPR of Free Radicals in Solids*, edited by A. Lund and M. Shiotani (Kluwer Academic, Dordrecht, 2003), p. 601.
 - ¹²J. N. Baillargeon, K. Y. Cheng, G. E. Hofler, P. J. Pearah, and K. C. Hsieh, *Appl. Phys. Lett.* **60**, 2540 (1992).
 - ¹³X. Liu, S. G. Bishop, J. N. Baillargeon, and K. Y. Cheng, *Appl. Phys. Lett.* **63**, 208 (1993).
 - ¹⁴S. Miyoshi, H. Yaguchi, K. Onabe, and R. Ito, *Appl. Phys. Lett.* **63**, 3606 (1993).
 - ¹⁵L. Bellaiche, Su-Huai Wei, and Alex Zunger, *Phys. Rev. B* **56**, 10 233 (1997).
 - ¹⁶W. Shan, W. Walukiewicz, K. M. Yu, J. Wu, J. W. Ager III, E. E. Haller, H. P. Xin, and C. W. Tu, *Appl. Phys. Lett.* **76**, 3251 (2000).
 - ¹⁷H. P. Xin, C. W. Tu, Yong Zhang, and A. Mascarenhas, *Appl. Phys. Lett.* **76**, 1267 (2000).
 - ¹⁸I. A. Buyanova, G. Pozina, J. P. Bergman, W. M. Chen, H. P. Xin, and C. W. Tu, *Appl. Phys. Lett.* **81**, 52 (2002).
 - ¹⁹H. Yonezu, *Semicond. Sci. Technol.* **17**, 762 (2002).
 - ²⁰K. Momose, H. Yonezu, Y. Fujimoto, Y. Furukawa, Y. Motomura, and K. Aiki, *Appl. Phys. Lett.* **79**, 4151 (2001).
 - ²¹I. Suemune, K. Uesugi, and T.-Y. Seong, *Semicond. Sci. Technol.* **17**, 755 (2002).
 - ²²K. Onabe, in *III-V Nitrides*, edited by F. A. Ponce, T. D. Montakas, I. Akasaki, and B. A. Monemar, *Mater. Res. Soc. Symp. Proc. No. 449* (Materials Research Society, Pittsburgh, 1997), p. 23.
 - ²³N. Q. Thinh, I. P. Vorona, I. A. Buyanova, W. M. Chen, S. Limpitjumnong, S. B. Zhang, Y. G. Hong, H. P. Xin, C. W. Tu, A. Utsumi, Y. Furukawa, S. Moon, A. Wakahara, and H. Yonezu, *Phys. Rev. B* **70**, 121201(R) (2004).
 - ²⁴N. Q. Thinh, I. P. Vorona, M. Izadifard, I. A. Buyanova, W. M. Chen, Y. G. Hong, H. P. Xin, and C. W. Tu, *Appl. Phys. Lett.* **85**, 2827 (2004).
 - ²⁵I. A. Buyanova, G. Yu. Rudko, W. M. Chen, H. P. Xin, and C. W. Tu, *Appl. Phys. Lett.* **80**, 1740 (2002).
 - ²⁶G. A. Baraff and M. Schluter, *Phys. Rev. Lett.* **55**, 1327 (1985).
 - ²⁷P. Blaha, K. Schwarz, G. K. H. Madsen, D. Kvasnicka, and J. Luitz, computer code WIEN2K, An Augmented Plane Wave + Local Orbitals Program for Calculating Crystal Properties, Karlheinz Schwarz, Technical Universität Wien, Austria, 2001.
 - ²⁸G. Kresse and J. Furthmüller, *Comput. Mater. Sci.* **6**, 15 (1996).
 - ²⁹F. Rong and G. D. Watkins, *Phys. Rev. Lett.* **58**, 1486 (1987).
 - ³⁰C. G. Van de Walle and P. E. Blöchl, *Phys. Rev. B* **47**, 4244 (1993).
 - ³¹M. Linde, S. J. Uftring, G. D. Watkins, V. Härle, and F. Scholz, *Phys. Rev. B* **55**, R10 177 (1997).
 - ³²C. Bozdog *et al.*, *Phys. Rev. B* **59**, 12 479 (1999).
 - ³³K. H. Chow and G. D. Watkins, *Phys. Rev. Lett.* **85**, 2761 (2000).
 - ³⁴G. D. Watkins and J. W. Corbett, *Phys. Rev.* **121**, 1001 (1961).
 - ³⁵T. A. Kennedy and M. G. Spencer, *Phys. Rev. Lett.* **57**, 2690 (1986).
 - ³⁶T. A. Kennedy, R. Magno, and M. G. Spencer, *Phys. Rev. B* **37**, 6325 (1981).
 - ³⁷J. M. Trombetta, T. A. Kennedy, W. Tseng, and D. Gammon, *Phys. Rev. B* **43**, 2458 (1991).
 - ³⁸T. Wimbauer *et al.*, *Phys. Rev. B* **58**, 4892 (1998).
 - ³⁹K. M. Lee, in *Defects in Electronic Materials*, edited by M. Stavola *et al.*, *Mater. Res. Soc. Symp. Proc. No. 104* (Material Research Society, Pittsburgh, 1988), p. 449.
 - ⁴⁰W. M. Chen and B. Monemar, *Phys. Rev. B* **40**, 1365 (1989).
 - ⁴¹W. M. Chen, B. Monemar, E. Jánzén, and J. L. Lindström, *Phys. Rev. Lett.* **67**, 1914 (1991).